Combust. Sci. and Tech., 1991, Vol. 77, pp. 189–202
Reprints available directly from the publisher
Photocopying permitted by license only

Temperature and Radiation of Diffusion Flames with Suppression

J. P. GORE *University of Maryland, Mechanical Engineering Department, College Park, MD 20742*

D. D. EVANS *National Institute of Standards and Technology, Center for Fire Research, Gaithersburg, MD 20899*

and B. J. McCAFFREY *University of Maryland, Baltimore County, Mechanical Engineering Department, Catonsville, MD 21228*

(Received June 7, 1990; in final form November 30, 1990)

Abstract—Temperature and radiation properties of 1–8 MW heat release rate methane/air jet diffusion flames without and with the addition of liquid water suppressant to the fuel stream are studied. The analysis includes an existing parabolic flow solver, in conjunction with the locally homogeneous flow approximation and the laminar flamelet concept. State relationships for methane + liquid water mixtures are calculated from species concentration measurements for methane flames without water added. The analyses are compared with previously published data. Tests for flames without water addition show the applicability of the analyses to the present flame scales. The results for flames with water addition indicate that finite rates of evaporation and separated flow effects need to be considered for accurate predictions at high water loading.

INTRODUCTION

Radiation and extinction of large turbulent jet flames is of interest in the evaluation of hazard to personnel resulting from oil and gas well blowouts. Motivated by this problem, experiments concerning the feasibility of extinguishment of large (100–200 MW; Evans and Pfenning, 1985) and medium (1–10 MW; McCaffrey, 1986, 1989) scale methane/air flames using water sprays have been conducted in the past.

Predictions of structure and radiation properties of laboratory scale methane flames (10–20 kW) have been reported by Jeng *et al.* (1984) and by Jeng and Faeth (1984a). These methods were applied to the prediction of temperature and radiation properties of large (100–200 MW) flames by Gore *et al.* (1986). In the past work, the predictions were restricted to methane/air flames without suppression.

The objective of the present work is to extend the analysis of flame structure and radiation to include the effects of water added to the fuel stream as a suppressant. As a first step, the two phase flow effects are treated using the locally homogeneous flow approximation described by Faeth (1988). Experimental data reported by McCaffrey (1986, 1989) are utilized to evaluate the results and to discuss the limitations of the approach.

Williams (1974, 1981) has presented a view, based on the extinction of thin laminar diffusion flamelets, that fire extinguishment is due to excessive heat loss to the rich and/or lean side of the flame. This heat loss could be enhanced by the presence of a suppressant or by large flame stretch. Thus, evaluation of heat loss to water and the subsequent decrease in flame temperature is important in understanding fire suppression. With water added to the fuel stream as a suppressant, the additional heat loss occurs as a result of increased heat of vaporization and sensible energy extracted from the flamelets. Therefore, the extinction mechanism is entirely thermal. Seshadri (1978) has verified this for diffusion flames burning above a liquid fuel surface in a counter-flow configuration.

In addition to decreasing the temperature, the evaporation of water increases the partial pressure of water vapor and may lead to an increase in the emissivity of the flame as discussed by McCaffrey (1989). The resulting effects on flame radiation levels therefore may not be negligible. The addition of water to the fuel stream also affects flame radiation by suppressing soot production. Fortunately, radiation from methane flames is dominated by the bands of stable molecular species such as carbon dioxide and water vapor (Jeng *et al.*, 1984) allowing the present treatment without the complications of soot chemistry.

Other factors, not considered in the locally homogeneous flow (LHF) approximation (Faeth, 1988) and the view of extinction summarized above (Williams, 1974, 1981) are the non-uniformity introduced by turbulent mixing in the high speed flow and differential diffusion of the liquid water suppressant and the gaseous (fuel, oxidizer and product) species. Due to these effects, flamelets at one location may be subjected to very high quantities of suppressant while flamelets at another location may not see any suppressant at all. These separated flow phenomena may have significant effects on the radiation and extinction properties due to their nonlinear dependence on flame cooling.

In this work, locally homogeneous flow is assumed in order to evaluate the baseline case of water added in the form of an idealized mist consisting of infinitesimally small water droplets. The effect of water addition is assumed to be purely thermal and finite rate reaction effects are neglected. As conditions close to flame extinction are approached, this is clearly not valid. However, this approach establishes a baseline case of practical importance for fire situations where combustion of the fuel with low radiation hazard is beneficial compared to fire extinction and subsequent discharge of unburnt fuel. The effects of finite rate chemistry can be assessed by comparing the measurements with predictions.

In the following, the experiments described in detail by McCaffrey (1986, 1989) are briefly summarized before discussing the present theoretical methods. The results concerning state relationships with water addition are presented next, followed by a comparison of measurements and predictions for turbulent flames without suppressant and then for those with added water spray. The paper concludes with a statement concerning the limitations of the present theoretical approach.

EXPERIMENTS

The experimental apparatus used by McCaffrey (1986, 1989) involved a 104 mm diameter main natural gas pipe with a pressure atomizing nozzle (PAN) mounted at the center at a depth of 59 mm from the exit as shown in Figure 1. At the exit, the pipe had a sudden contraction to 32 mm diameter. The twin fluid pressure atomizing nozzle was supplied with liquid water in the central portion and atomizing methane driver admitted at approximately 150 KPa to the annulus. Two different exit geometries were considered (sharp-edged orifice or straight cut hole). However, the differences in the measurements were within the measurement uncertainties (McCaffrey, 1986, 1989). Therefore, no distinction between the two nozzle geometries has been made in the present paper. The nozzle was located at the bottom of a 5 m deep underground pit. Air entered the pit from large openings at the surface.

Water and atomizing methane were metered using rotameters. The main methane flow was metered using a laminar flow element. The temperature measurements involved six chromel–alumel thermocouple junctions formed from 0.5 mm diameter wire mounted at 0.5, 1, 2, 3, 4 and 5 meters from the injector exit. The radiative heat

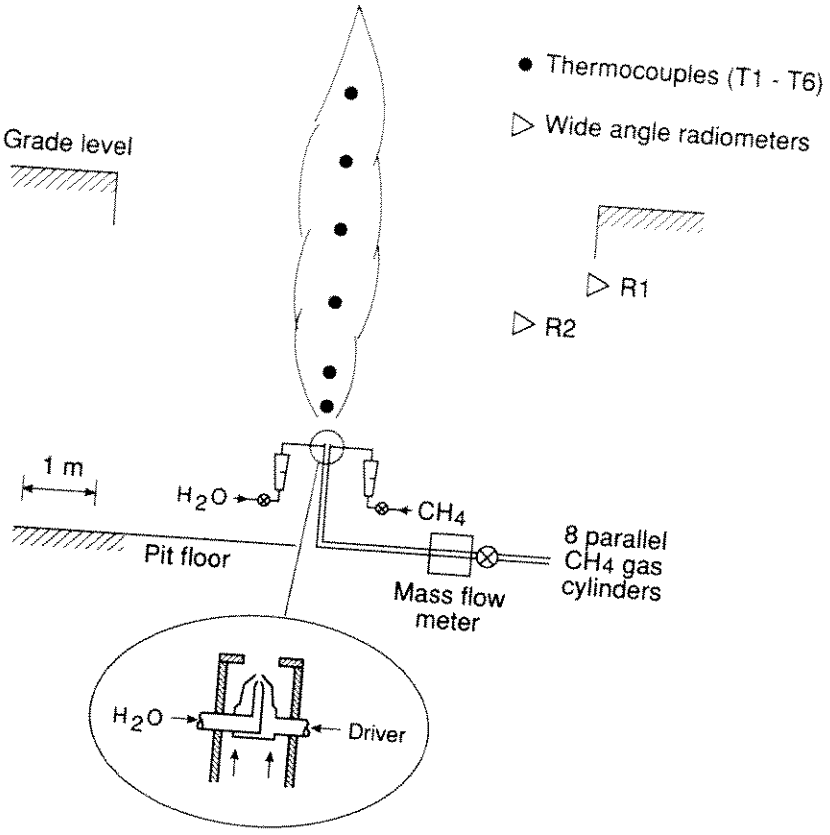

FIGURE 1 Sketch of the experimental apparatus.

flux detectors involved two wide angle (150° view angle) broad band radiometers (Medtherm Corp.) mounted at: (1) 2.6 m radius and 1.9 meters height from the injector exit and (2) 3.5 m radius and 2.5 meters height from the injector exit. The radiometer locations were selected somewhat arbitrarily to sample representative radiative heat flux distribution around the flames.

The nominal heat release rates for the operating conditions selected by McCaffrey (1986, 1989) varied between 1–10 MW. These conditions yield fully turbulent (exit Reynolds numbers = $Re = u_0 d/\nu = 30{,}000$–$500{,}000$, where u_0 is the equivalent exit velocity calculated from mass flow rates, d is the injector diameter at the exit and ν is the kinematic viscosity) flow at the jet exit. The flames are momentum dominated in the near-injector region but buoyancy influences the flame height due to reduction in local momentum of the jets by mixing. According to the criterion of Becker and Liang (1978), the flames are in the intermediate regime (Richardson number = $Ri = ad/u_0^2 = 0.000014$–0.00012, where a is the gravitational acceleration). Many of the flames were lifted from the injector exit since no pilots or other methods of flame attachment were provided.

The tests were begun by first lighting a small flame of methane and then increasing the fuel mass flow until the desired operating condition was reached. During the suppression tests, two minutes after the establishment of the desired gas flow condition, the water flow was started and increased in desired steps until the limiting flow

was reached. This allowed collection of temperature profile data and radiative heat flux data for the baseline methane flames without suppression and also for flames with different water/methane mass ratios.

THEORETICAL METHODS

Since radiation from methane flames is dominated by gaseous bands (Jeng *et al.*, 1984), the effects of water addition are assumed to be purely thermal. Thus the state relationships for flames with water added to the fuel stream are constructed using species concentration data for pure methane flames and adding liquid water to the fuel in an appropriate amount as an inert species. The effect of water is to reduce the temperature by extracting the heat of vaporization and sensible heat. Changes in temperature caused by water addition will clearly affect the rates of chemical reactions. However, as a first step, the reaction rates are assumed to be much faster than the mixing rates. The validity of this assumption for the present test conditions can be examined using the results.

It is noted that the reduced temperatures caused by the addition of water will affect the details of the flame structure significantly. The present approximation is for the purpose of calculating flame radiation only. Trace species formation will be affected significantly by finite reaction rates. As discussed before, the effects of these species (including soot) on flame radiation properties can be neglected for the present methane flames.

It is assumed that water is added to the fuel stream in the form of very fine mist so that the instantaneous velocities of the two phases are identical at the exit and that differential diffusion effects between the gas phase and water drops are negligible. This corresponds to the locally homogeneous flow (LHF) approximation described by Faeth (1988). Effects of liftoff of flames from the injector exit are neglected since the liftoff heights are small compared to the flame height and also due to the considerable uncertainty concerning the structure of lifted flames (Pitts, 1988). Potential effects of liftoff can be assessed based on the results for methane flames without suppression.

The density of the material leaving the injector is increased due to the presence of liquid water reducing the air entrainment rates for the jet. The velocity of the jet leaving the injector, u_0, is calculated using a mass balance and assumed to be uniform at the jet exit. In addition to initial density and velocity distributions, mixture fraction, turbulent kinetic energy, mixture fraction fluctuations and dissipation of turbulent kinetic energy are needed at the initial station. Approximate initial conditions are specified similar to past practice (Jeng and Faeth, 1984a, b; Gore *et al.*, 1986; Faeth, 1988). Once the distributions of the above variables in the flow are known, mean scalar properties needed for calculating radiative heat flux such as temperature and species concentrations are obtained from the state relationships using averaging based on a clipped Gaussian probability density function (Jeng and Faeth, 1984a, b).

State Relationship in the Presence of Liquid Water

Bilger (1977) proposed the laminar flamelet concept based on the observation that measurements of gaseous species concentrations in laminar flames without suppressant are functions only of mixture fraction. As long as the effect of water addition is thermal, this idea can be extended to flames with water suppressant as described in the following.

Measurements of gaseous species concentrations for laminar flames burning meth-

ane in air (Tsuji and Yamaoka, 1969) show that the global reaction (considering only the species whose mole fractions are above 0.01 as important for the present calculations) can be written as:

$$CH_4 + bO_2 + 3.76bN_2 = x_{CH_4}CH_4 + x_{N_2}N_2 + x_{CO_2}CO_2 + x_{H_2O}H_2O + x_{CO}CO + x_{H_2}H_2. \quad (1)$$

Where "x_i" are the number of moles on the product side for species "i", for 1 mole of methane on the reactant side, calculated from the species concentration measurements and C and H atom balances. Moles of oxygen on the reactant side per mole of methane are denoted by "b" and are determined from the local mixture fraction. In order to construct the state relationships for methane + liquid water burning with air, x_w moles of liquid water are added to the fuel stream per mole of methane. Since the effects of this addition are only thermal, the chemical reaction now becomes:

$$CH_4 + x_wH_2O(l) + bO_2 + 3.76bN_2 = x_{CH_4}CH_4 + x_{N_2}N_2 + x_{CO_2}CO_2 + cx_{H_2O}H_2O(v) + dx_{H_2O}H_2O(l) + x_{CO}CO + x_{H_2}H_2. \quad (2)$$

The moles of water added per mole of CH_4 are calculated from the operating conditions. The additional unknown in Eq. (2) is the moles of water in the liquid form in the products. Under the present approximations, the mole fraction of water vapor is determined by assuming thermodynamic equilibrium for the combustion products. Thus the mole fraction of water in the vapor phase in the presence of liquid water is:

$$x_{H_2O}(v) = P_v(T) \quad (3)$$

where x_{H_2O} is the mole fraction of water vapor and $P_v(T)$ is the equilibrium vapor pressure of water at temperature T. The temperature of the products must be known to find the vapor pressure in Eq. (3). The temperature is obtained using the first law of thermodynamics with a fixed radiative heat loss fraction X_R for a given water addition. This can be summarized as:

$$(1 - X_R)(h^0_{f,CH_4} + x_w h^0_{f,H_2O} - \Sigma x_i h^0_{fi}|_P) = \Sigma x_i h_i|_P, \quad (4)$$

where the summation is over all species on the product side (denoted by $|_P$) of Eq. (2) and x_i denote the moles of species i and h^0_{fi} is the heat of formation of species i with elements on the reactant side assumed to be in the reference state. Eq. (3) and (4) must be solved simultaneously for obtaining the partial pressure of water vapor and the temperature of the products. The mole fractions of individual product species are then obtained using atom balance on Eq. (2).

The density of the two phase mixture is obtained noting that the specific volumes of the two phases are additive:

$$v = Y_g v_g + Y_l v_l, \quad (5)$$

where v is the specific volume of the mixture and Y_g is the mass fraction of all species in the gas or vapor phase (specific volume v_g) and Y_l is the mass fraction of the liquid water (specific volume v_l).

The mixture fraction of each point in the state relationship for a methane + water mixture is calculated by modifying the mixture fractions in the gaseous fuel state relationship to include the effect of water addition:

$$f_1 = f(x_w W_w / W_{CH_4} + 1)/(1 + f x_w W_w / W_{CH_4}), \quad (6)$$

where f is the mixture fraction in the original state relationship, f_1 is the mixture fraction in the state relationship with water addition, and W_i are the molecular weights of water and methane for $i = w$ or CH_4.

The gas phase mole fractions of all the species are affected due to the addition of water. These are calculated from the RHS of Eq. (2). Thus the mole fraction of water vapor at all mixture fractions increases due to water addition while the mole fractions of all other gaseous species decrease.

Once the state relationships for the fuel–water mixture are calculated as described above, the procedure for calculation of flame structure and radiative heat fluxes is similar to the one used in past studies (Jeng and Faeth, 1984a, b; Jeng *et al.*, 1984; and Gore *et al.*, 1986). The flame structure calculations involve solution of governing equations for mean mass, momentum, mixture fraction, turbulent kinetic energy and its dissipation and mean square mixture fraction fluctuations using the GENMIX algorithm of Spalding (1977). A Favre averaged formulation described by Bilger (1976) as modified by Jeng and Faeth (1984a) was used. All of the constants in the turbulence model were unchanged from the values used by Jeng and Faeth (1984a).

The radiation calculations utilized a modified version (Jeng and Faeth, 1984b) of the discrete transfer method of Lockwood and Shah (1981). The RADCAL algorithm of Grosshandler (1980) as modified by Jeng *et al.* (1984) was used in the calculation of radiation intensities along discrete paths. The near infrared (1–10 microns wavelength) bands of CO_2, H_2O, CH_4 and CO were included in the calculations.

RESULTS AND DISCUSSION

Flames without Water Addition

As discussed before, the experimental procedure allowed the collection of data for flames burning methane without the addition of water suppressant as a baseline. In the following, these data are used to compare the baseline predictions first before considering the effects of water addition. Present theoretical methods have been evaluated in the past for laboratory flames (around 20 kW heat release, Jeng and Faeth, 1984) and very large scale flames (around 200 MW heat release, Gore *et al.*, 1986). The present tests allow an evaluation of the scaling effects using intermediate size flames (heat release rates between 1–10 MW).

Figure 2 shows measurements and predictions of temperature along the axis of a 4.6 MW flame burning methane without water suppressant. The symbols represent averages of data from several runs. The data are not corrected for radiation heat loss from the thermocouples and conduction losses to leads and guide wires. These losses are estimated to be 200–400 K. The predictions are in reasonable agreement with the data considering limitations of the present analysis, measurement uncertainty and effects of flame liftoff. The agreement between data and predictions is similar to that of earlier analyses for attached flames suggesting that the effects of liftoff are not significant for the present operating conditions.

Radiative heat flux measured by two radiometers facing the axis of the flames are plotted in Figure 3. The radiometer positions are arbitrary and therefore representa-

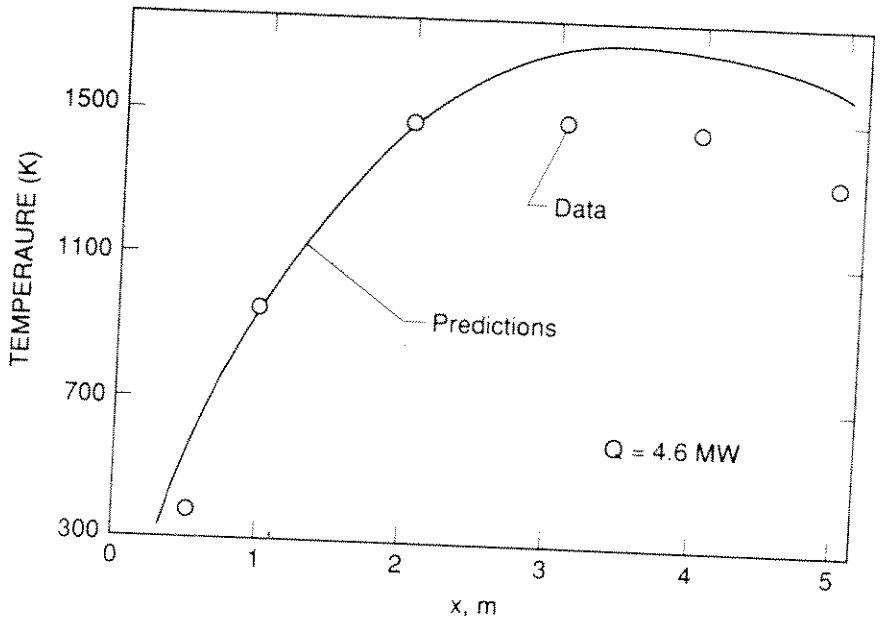

FIGURE 2 Temperature distribution along the axis of 4.6 MW methane flames.

tive of the surrounding locations. The positions utilized by McCaffrey (1986 (also 1989)) are given in the inset of Figure 3. Predictions of the radiative heat flux using the discrete transfer method are also plotted in Figure 3. The radiative heat flux is plotted as a function of the nominal heat release rate of the flames. As seen from Figure 3, the agreement between predictions and measurements is good for the range (0.5–7 MW) of heat release rates considered. The slope of the heat flux versus heat release rate curves changes due to the flame length and width variations introduced by the effects of buoyancy and momentum (characterized by the Richardson number). It is particularly encouraging that the analysis captures the changes in the slope observed from the data. The predictions are consistently somewhat lower than the measurements due to possible effects of continuum radiation from soot and effects of turbulence radiation interactions (Gore *et al.*, 1986). However, the differences are well within other uncertainties in predictions and measurements. The radiative heat flux data and predictions also indicate that effects of liftoff on this global, integrated property can be neglected in engineering calculations.

Effect of Water Addition on State Relationships

The effects of water addition on the state relationships are described next. Figure 4 is a plot of mole fractions of water vapor as a function of equivalence ratio (which is a single valued function of mixture fraction) for no water addition and for four water mass loading ratios ($\dot{m}_{H_2O}/\dot{m}_{CH_4}$). For all the water loadings shown in Figure 4, the water vapor mole fractions are higher than the baseline case. At a water loading ratio of 3, the peak mole fraction of water vapor is over 0.4 at an equivalence ratio of 2. The peak occurs on the fuel rich side because the liquid water is added to the fuel and the contribution from its vaporization is much higher for this loading ratio than the contribution from the oxidation of methane. The water vapor mole fraction decreases sharply for equivalence ratios greater than 2.0 since the additional water

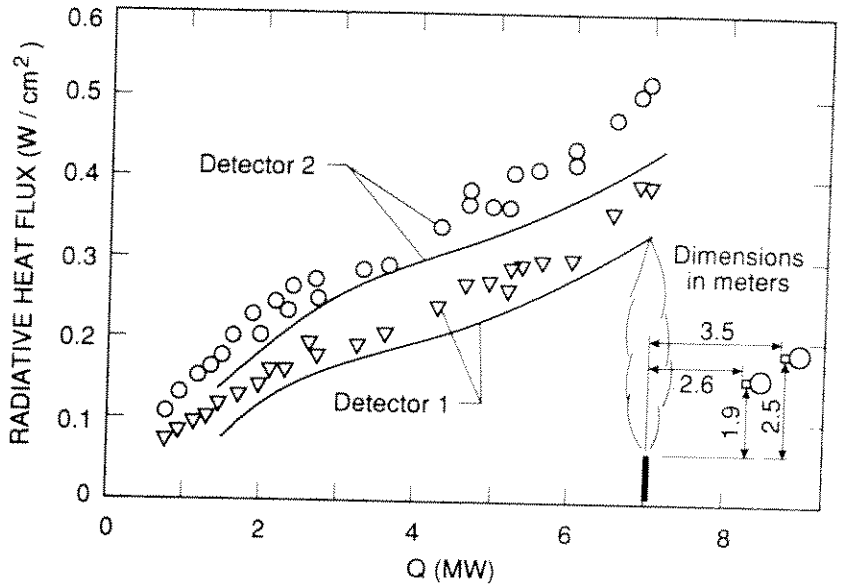

FIGURE 3 Radiative heat flux as a function of heat release rate for methane flames in the range 0.5 MW to 8 MW.

remains in the liquid form due to lower temperatures attained by evaporation as discussed later on. For a water loading ratio of 2.0, the peak water vapor mole fractions occur at an equivalence ratio of 3.0. As the water loading is decreased further, the state relationships develop two peaks—one corresponding to the stoichiometric point and another corresponding to the maximum vapor phase equilibrium mixture. In fact at a water loading ratio of 0.46, the water vapor mole fraction is highest at an equivalence ratio of 10.

The mole fractions of water vapor have an effect on the absorption coefficient in the water vapor bands as discussed by McCaffrey (1986, 1989). In particular the relatively low decrease in radiation heat fluxes was attributed to the enhanced flame emissivity based on an early evaluation of the data. However, the overall absorption coefficient also depends on the concentrations of CO_2 and on temperature and may vary in a complicated way as water loading is increased. The results of the present calculations will provide an indirect check on the variation of the absorption coefficient with water loading.

The state relationships for the mole fractions of liquid water are plotted in Figure 5. These show maximum liquid water at the highest fuel equivalence ratio (10 in Figure 5) for all water loadings. The liquid water mole fraction decreases as the fuel + water mixes with the combustion gases (equivalence ratio decreases) for all loadings. Figure 5 shows that liquid water reaches nearer the stoichiometric flame surface as the water loading is increased. It appears that at a loading ratio of approximately 3, liquid water penetrates the active reaction zone (estimated to be between equivalence ratios of 0.4 and 2 based on the analysis of Bilger *et al.*, 1990) explaining the critical loading for flame extinction. As liquid water penetrates to locations near the flame surface, the heat loss from the flame to the fuel side (when water is added to the fuel stream) increases continuously. At water loadings near extinction the heat loss would be such that chemical reactions could no longer be sustained. As this limit is approached the present treatment is no longer valid since

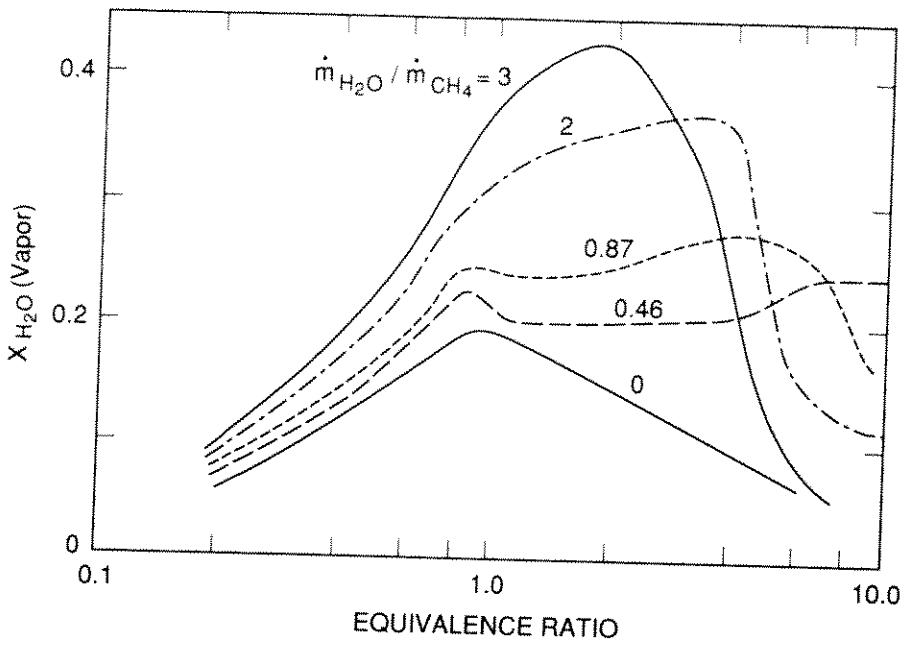

FIGURE 4 State relationships for water vapor mole fraction for methane flames with water suppressant.

effects of finite rate chemistry become predominant. The enhanced heat loss can be studied using the temperature state relationships discussed in the following.

Figure 6 shows the state relationships for temperature. The radiative heat loss fraction is assumed to be constant at 0.18 in calculating these state relationships. It was found that the results are somewhat insensitive to this parameter. Thus the coupling between radiative heat losses and the flow enthalpy has been neglected similar to past practice. The state relationships for temperature without water addition show a peak temperature of approximately 2000 K near the stoichiometric point. As the water loading is increased, the peak temperature decreases. At low water loadings, all the water is evaporated in the very rich regions. In regions where liquid water exists, the temperature is held to relatively low values as dictated by the vapor pressure curve. At equivalence ratios leaner than the point at which all water evaporates, the temperature rises rapidly up to the stoichiometric equivalence ratio and then decreases on the fuel lean side. The peak temperature decreases to approximately 1400 K at a water loading ratio of 2 and to 1300 K at a water loading ratio of 3. These temperatures are close to where the rates of most chemical reactions are reduced to such small values that in the presence of heat loss, extinction occurs. The rate of heat loss can be assessed based on the gradient of temperature near the peak. As seen from Figure 6, as the water loading is increased, the heat loss to the fuel rich side increases significantly while the heat loss to the fuel lean side decreases only slightly.

The effect of water addition on the mole fractions of CO_2 is plotted in Figure 7. Two representative water loadings together with the baseline zero water loading case are shown. As seen from Figure 7, the mole fraction of CO_2 decreases for all equivalence ratios as the water loading is increased. Thus although the flame absorption coefficient would increase due to additional water vapor, it would decrease due to a reduction in CO_2 mole fraction. The net effect is complicated since the absorption coefficient is also a function of temperature.

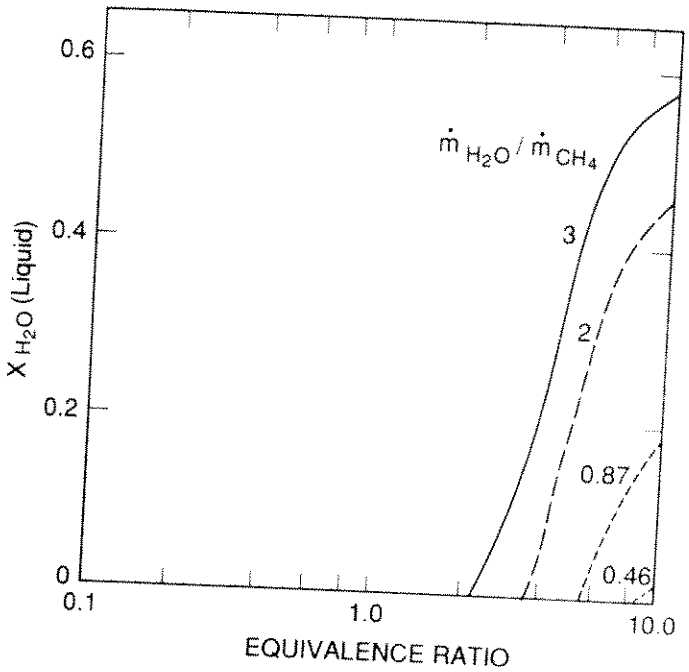

FIGURE 5 State relationships for liquid water mole fraction for methane flames with water suppressant.

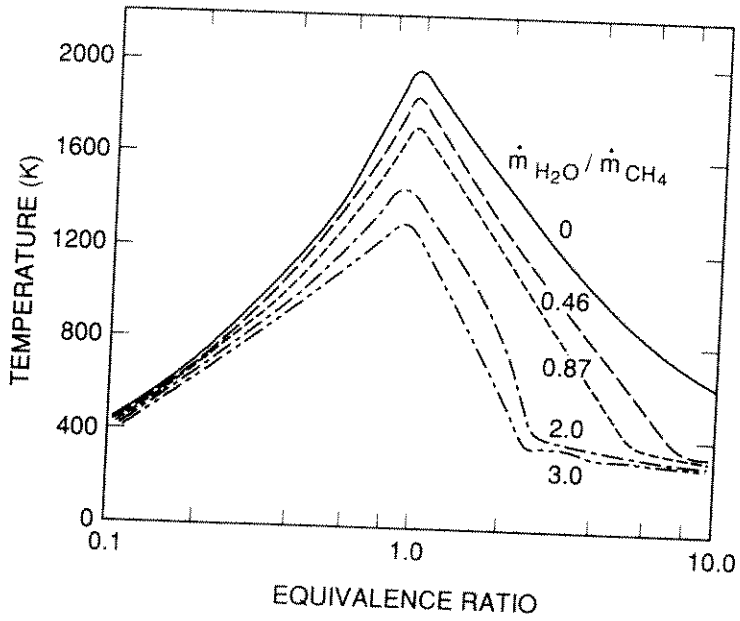

FIGURE 6 State relationships for temperature for methane flames with water suppressant.

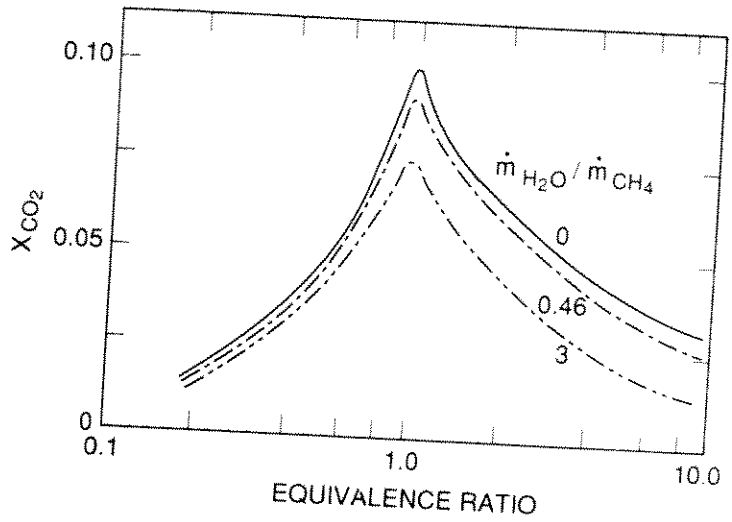

FIGURE 7 State relationships for CO_2 mole fractions for methane flames with water suppressant.

Effect of Water Addition on Turbulent Flames

The effect of water addition on the turbulent flames is studied by examining the measurements and predictions of temperature at 4 meters from the injector exit (a representative location) as a function of the water loading ratio for the 4.6 MW flame. This location remains approximately the position of the peak temperature based on both the data and the predictions. This is a combined effect of the reduced air requirements for complete combustion, increased initial momentum and decreased buoyancy on air entrainment with increased water loading. It is encouraging that the analysis predicts the combined effects of these complex phenomena.

Figure 8 shows the variation in the measurements and predictions of temperature as a function of water loading. The difference between measurements and predictions is approximately 400 K for zero water loading. As the water loading increases, the predicted temperature decreases faster than the measurements such that the difference between the two is reduced to less than 100 K implying that the predicted temperatures are decreasing faster with increasing water loading than the thermocouple measurements. Thus the reduction in temperature is overpredicted by the analysis. This is probably due to the assumption of complete evaporation. In the experiment, complete evaporation was not realized due to imperfect atomization and finite evaporation rates as suggested by some amount of water (unfortunately not measured) observed on the floor after each test. A second reason for the increased temperature drop is associated with the reduced radiative heat losses that are not considered in the construction of the temperature state relationships. However, this effect was found to be small based on a parametric analysis of the radiation calculations. Thus the discrepancies appear to be associated with the incomplete evaporation of water within the spray. This effect can only be addressed by considering separated flow models with finite evaporation rates. The temperature of the flames with water addition appears to be overestimated although to a lesser degree than that of the flames without water addition based on Figure 8. Based on this, the radiative heat flux to surrounding locations, which was predicted correctly for the flames without water addition, is expected to be underestimated for the flames with water addition.

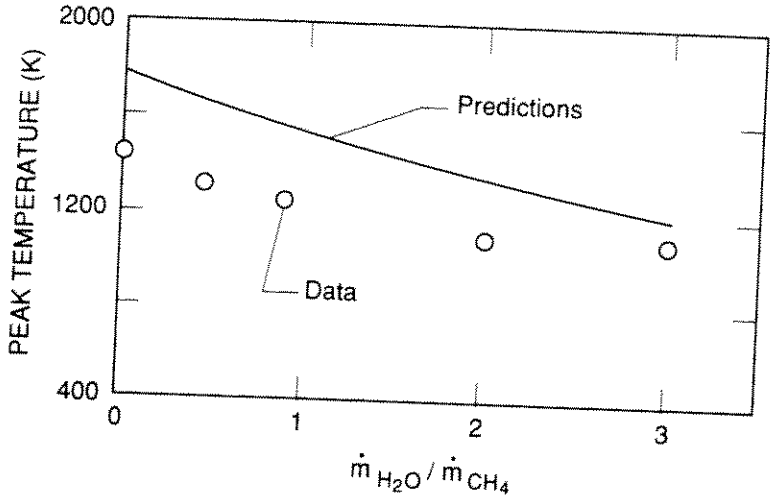

FIGURE 8 Peak temperature as a function of water loading for turbulent methane flames with water suppressant.

Figure 9 shows the measurements and predictions of radiative heat flux, averaged between the two locations shown in Figure 3, as a function of the water loading. As the water loading increases the difference between measurements and predictions increases progressively. At a water loading of 0.46, the decrease in radiative flux is predicted correctly. It appears that the temperature is underestimated because of the assumption of complete evaporation of water. Another reason for the discrepancies in the measurements and predictions of radiative heat fluxes could be that the liquid water is not transported to the edge of the jet together with the gaseous fuel. Thus, near the edge flamelets may be established with relatively low water loading while the central core may contain high water loading with near extinction flamelets. Visual observations of the flames with water addition show a white core of liquid towards the center surrounded by blueish flamelets on the outside qualitatively supporting this idea. Separated flow calculations that allow for finite interphase transport rates described by Faeth (1988) are needed to address this difficulty. It is noted that the discrepancies increase with increasing water loading supporting this idea.

The present calculations account for the increased water vapor concentrations and the resulting increase in the flame gas emissivity. However, the results shown in Figure 9 suggest that the increased emissivity does not compensate for the reduced temperatures and the predicted radiative heat flux decreases considerably with water loading. It is noted that the predictions shown in Figure 9 fortuitously agree with the T_{CL}^4 (where T_{CL} is the center line temperature with water addition normalized by that without water addition) profiles plotted by McCaffrey (1989). Temperature ratios, similar to T_{CL}, used in the present calculations, vary over a wide range as shown in Figure 6. Besides, calculations for higher detector locations showed lower temperature sensitivity than T_{CL}^4.

It is noted that if the rates of reaction had decreased significantly (contrary to the present assumptions) leading to lower than expected temperatures and product species concentrations, then the radiative heat flux would have been overestimated. The data show that as far as quantities needed for the prediction of flame radiation are concerned, the reaction rates are not limiting even at relatively high water loadings. This is also supported by the higher (compared to predictions) measured

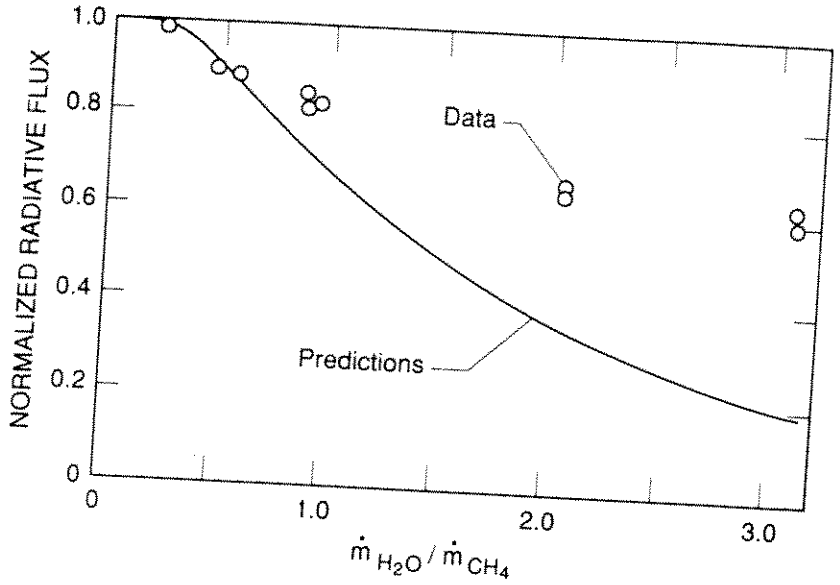

FIGURE 9 Radiative heat flux for methane flames with water suppressant.

temperatures. However, it must be added that, details of the flame structure will be substantially different and production of pollutant species will be significantly altered by the reduced temperature. Treatment of the effects of finite rate evaporation and separated flow effects appears to be the next logical step in the analysis.

CONCLUSIONS

The conclusions that can be drawn from the present study can be sumarized as follows:

(1) Baseline tests for pure methane indicate that existing flame structure and radiation analysis for turbulent jet flames can be applied over a wide range of flame scales. For engineering calculations, the effects of flame liftoff also appear to be small.

(2) For the present test conditions, the laminar flamelet method can be extended to flames with water addition to the fuel stream for conditions away from extinction for the purpose of calculating flame radiation.

(3) For higher water loadings, the effects of finite rate evaporation and also differential transport between the gas and liquid phases are important. Attention needs to be focussed on these topics.

ACKNOWLEDGEMENT

This research was sponsored by the United States Department of Commerce, National Institute of Standards and Technology, Center for Fire Research, Gaithersburg, MD 20899, with Dr. D. D. Evans serving as Scientific Officer. The experiments were performed at the Center for Fire Research with funding from the Minerals Management Service of the United States Department of Interior with Mr. Ed Tennyson of MMS serving as the Scientific Officer.

REFERENCES

Becker, H. A. and Liang, D., (1978) Visible Length of Vertical Free Turbulent Diffusion Flames, *Comb. Flame*, **32,** 115–137.

Bilger, R. W., (1976) Turbulent Jet Diffusion Flames, *Prog. Energy Combust. Sci.*, **1,** 87–109.

Bilger, R. W., (1977) Reaction Rates in Diffusion Flames, *Comb. Flame*, **30,** 277–284.

Bilger, R. W., Starner, S. H., and Kee, R. J., (1990) On Reduced Mechanisms of Methane-Air Combustion in Nonpremixed Flames, *Comb. Flame*, **80,** (2) 135–149.

Evans, D. D. and Pfenning, D. B., (1985) Water sprays suppress gas-well blowout fires, *Oil and Gas J.*, **83,** (17) 80–86.

Faeth, G. M., (1988) Mixing, Transport and Combustion in Sprays, *Prog. Combust. Sci. Tech.*, **13,** 293–345.

Gore, J. P., Faeth, G. M., Evans, D. D., and Pfenning, D. B., (1986) Structure and Radiation Properties of Large Scale Natural Gas/Air Diffusion Flames, *Fire and Materials*, **10,** 161–169.

Gore, J. P., Evans, D. D., and McCaffrey, B. J., (1988) Temperature and Radiation Properties of Large Methane/Air Flames with Water Suppression, *Proceedings of the Twenty-First Fall technical Meeting of the Eastern States Section*, The Combustion Institute, Pittsburgh, PA., pp. 60.1–60.4.

Grosshandler, W. L., (1980) Radiative Heat Transfer in Nonhomogeneous Gases: A Simplified Approach, *Int. J. Heat and Mass Trans.*, **23,** 1447–1459.

Jeng, S. M., Lai, M. C., and Faeth, G. M., (1984) Nonluminous Radiation in Turbulent Buoyant Axisymmetric Flames, *Combust. Sci. Tech.*, **40,** 41–53.

Jeng, S. M. and Faeth, G. M., (1984a) Species Concentrations and Turbulence Properties of Buoyant Methane Diffusion Flames, *J. Heat Trans.*, **106,** 721–727.

Jeng, S. M. and Faeth, G. M., (1984b) Radiative Heat Fluxes Near Turbulent Buoyant Methane Diffusion Flames, *J. Heat Trans.*, **106,** 886–888.

Lockwood, F. C. and Shah, N. B., (1981) A New Radiation Solution Method for Incorporation in General Combustion Prediction Procedures, *Eighteenth Symposium (International) on Combustion*, The Combustion Institute, Pittsburgh, PA, pp. 1405–1414.

McCaffrey, B. J., (1986) Momentum Diffusion Flame Characteristics and the Effects of Water Spray, NBSIR 86-3442, National Institute of Standards and Technology, Gaithersburg, MD.

McCaffrey, B. J., (1989) Momentum Diffusion Flame Characteristics and the Effects of Water Spray, *Combust. Sci. and Tech.*, **63,** 315–335.

Pitts, W. M., (1988) Assessment of Theories for the behavior and Blowout of Lifted Turbulent Jet Diffusion Flames, *Twenty Second Symposium (International) on Combustion*, The Combustion Institute, Pittsburgh, PA., 809–816.

Seshadri, K., (1978) Structure and Extinction of Laminar Diffusion Flames Above Condensed Fuels with Water and Nitrogen, *Comb. Flame*, **33,** 197–215.

Spalding, D. B., (1977) *GENMIX: A General Computer Program for Two Dimensional Parabolic Phenomena*, Pergamon Press, Oxford.

Tsuji, H. and Yamaoka, I., (1969) The Structure of Counterflow Diffusion Flames in the Forward Stagnation Region of a Porous Cylinder, *Twelfth Symposium (International) on Combustion*, The Combustion Institute, Pittsburgh, PA, pp. 997–1005.

Williams, F. A., (1981) A Review of Flame Extinction, *Fire Safety Journal*, **3,** 163–175.

Williams, F. A., (1974) A Unified View of Fire Suppression, *J. Fire and Flammability*, **5,** (1) 54–63.